Accepted Manuscript

Evaluation of branched GDGTs and leaf wax *n*-alkane δ ^{2}H as (paleo) environmental proxies in East Africa

Sarah Coffinet, Arnaud Huguet, Nikolai Pedentchouk, Laurent Bergonzini, Christine Omuombo, David Williamson, Christelle Anquetil, Martin Jones, Amos Majule, Thomas Wagner, Sylvie Derenne
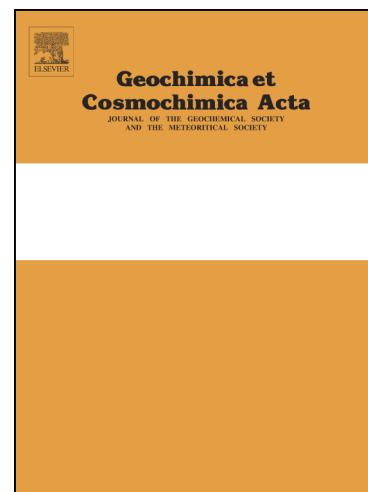
Please cite this article as: Coffinet, S., Huguet, A., Pedentchouk, N., Bergonzini, L., Omuombo, C., Williamson, D., Anquetil, C., Jones, M., Majule, A., Wagner, T., Derenne, S., Evaluation of branched GDGTs and leaf wax *n*-alkane δ ^{2}H as (paleo) environmental proxies in East Africa, *Geochimica et Cosmochimica Acta* (2016), doi: http://dx.doi.org/10.1016/j.gca.2016.11.020

Evaluation of branched GDGTs and leaf wax *n*-alkane δ²H as (paleo) environmental proxies in East Africa

Sarah Coffinet[a1], Arnaud Huguet[a], Nikolai Pedentchouk[b], Laurent Bergonzini[c], Christine Omuombo[d], David Williamson[e], Christelle Anquetil[a], Martin Jones[f], Amos Majule[g], Thomas Wagner[h], Sylvie Derenne[a]

[a]*Sorbonne Universités, UPMC Univ Paris 06, CNRS, EPHE, UMR 7619 METIS, 4 place Jussieu, 75252 Paris cedex 05, France*
[b]*School of Environmental Sciences, University of East Anglia, Norwich Research Park, Norwich, NR4 7TJ, United Kingdom*
[c]*Université Paris Saclay, UPS Univ Paris 11, CNRS, UMR 8148 GEOPS, rue du belvédère, Bât 504, 91405 Orsay cedex, France*
[d]*Department of Geology, University of Nairobi, Chiromo Campus, P.O. Box 30197, 00100 Nairobi, Kenya*
[e]*Institut de Recherche pour le Développement, Sorbonne Universités, UPMC Univ Paris 06, MNHN, CNRS, UMR 7159 LOCEAN, Centre IRD France Nord, F-93143, Bondy cedex, France*
[f]*Newcastle University, School of Civil Engineering and Geosciences, Newcastle-upon-Tyne, NE1 7RU, United Kingdom*
[g]*Institute of Resource Assessment, University of Dar Es Salaam, P.O. Box 35097, Dar Es Salaam, Tanzania*
[h]*Heriot-Watt University, Lyell Centre for Earth and Marine Science and Technology, School of Energy, Geoscience, Infrastructure and Society (EGIS), Edinburgh, EH14 4AS, United Kingdom*

Corresponding author email address: scoffinet@marum.de ; +49 421 218 65740

Abstract

The role of mountain evolution on local climate is poorly understood and potentially underestimated in climate models. One prominent example is East Africa, which underwent major geodynamic changes with the onset of the East African Rift System (EARS) more than 250 Myr ago. This study explores, at the regional East African scale, a molecular approach for terrestrially-based paleo-climatic reconstructions that takes into account both changes in temperature and in altitude, potentially leading to an

1   Present address: MARUM – Center for Marine Environmental Sciences, University of Bremen, Leobener Str., 28359 Bremen, Germany

34   improved concept in paleo-climatic reconstructions. Using surface soils collected along

35   pronounced altitudinal gradients in Mt. Rungwe (n=40; Southwest Tanzania) and Mt.

36   Kenya (n=20; Central Kenya), we investigate the combination of 2 terrestrial proxies, leaf

37   wax n-alkane δ^2H (δ^2H_{wax}) and branched glycerol dialkyl glycerol tetraether (br GDGT)

38   membrane lipids, as (paleo) elevation and (paleo) temperature proxies, respectively. At

39   the mountain scale, a weak link between δ^2H_{wax} and altitude ($R^2 = 0.33$) is observed at

40   Mt. Kenya, but no relationship is observed at Mt. Rungwe. It is likely that additional

41   parameters, such as decreasing relative humidity (RH) or vegetation changes with

42   altitude, are outcompeting the expected ^2H-depletion trend along Mt. Rungwe. In

43   contrast, br GDGT-derived absolute mean annual air temperature (MAAT) and

44   temperature lapse rate (0.65 °C/100 m) for both mountains are in good agreement with

45   direct field measurements, further supporting the robustness of this molecular proxy for

46   (paleo) temperature reconstructions. At the regional scale, estimated and observed δ^2H

47   data in precipitation along 3 mountains in East Africa (Mts. Rungwe, Kenya and

48   Kilimanjaro) highlight a strong spatial heterogeneity, preventing the establishment of a

49   regional based calibration of δ^2H_{wax} for paeloaltitudinal reconstructions. Different from

50   that, an improved regional soil calibration is developed between br GDGT distribution

51   and MAAT by combining the data from this study (Mts. Rungwe and Kenya) with

52   previous results from East African surface soils along Mts. Kilimanjaro (Tanzania) and

53   Rwenzori (Uganda). This new regional calibration, based on 105 samples, improves both

54   the R^2 (0.77) and RMSE (root mean square error; 2.4 °C) of br GDGT-derived MAAT

55   over the global soil calibrations previously established ($R^2 = 0.56$; RMSE = 4.2 °C) and

56   leads to more accurate (paleo) temperature reconstructions in the region.

57

1. Introduction

59   The East African Rift System (EARS) is one of the best examples of an active rift

60   system. The initial rifting in the area dates back to the Permo-Triassic and Cretaceous

61   (Macgregor, 2015). The development of this complex system with several phases of

62   rifting dramatically changed the East African landscape. Yet its potential influence on the

63   vegetation and local and African climate is hardly constrained. Previous modelling

64   (Sepulchre et al., 2006) postulated that the rise of the EARS should have greatly

65   contributed to the long term aridification of East Africa. However, these simulations only

66   compared 2 extreme scenarios: (i) no elevation and (ii) high elevation − reflecting the

67   lack of a well constrained history of the EARS rise. Moreover, paleo-climate

68   reconstructions in East Africa have long been hampered by 2 challenges: (i) traditional

69   hydrological proxies, such as lake level studies, are influenced not only by changes in the

70   amount of precipitation but also by ambient temperature; (ii) temperature changes are

71   poorly constrained because few sedimentary proxies are sensitive enough to accurately

72   record the small scale temperature variations in tropical lakes (*Verschuren et al., 2009*).

73   Recently, novel proxies were developed based on the analysis of fossil organic

74   compounds containing environmental information in their structures. Notably, leaf wax

75   n-alkane δ^2H (δ^2H_{wax}) was proposed as a (paleo) elevation proxy (Jia et al., 2008) while

76   branched glycerol dialkyl glycerol tetraether (br GDGT) membrane lipids are

77   increasingly used as a (paleo) temperature proxy (Weijers et al., 2007). The combined use

78   of these 2 proxies could thus help to better constrain the relationships between

79   topography and climate in East Africa.

80   Long chain *n*-alkanes are produced primarily by higher terrestrial plants (Eglinton

81   and Hamilton, 1967) and their ^{2}H/^{1}H ratio, typically expressed as δ²H$_{wax}$, is linked with

82   the ^{2}H/^{1}H ratio of the plant water source (e.g. Sauer et al., 2001). Because *n*-alkanes are

83   well preserved in the geological archives (Eglinton and Eglinton, 2008) and their

84   hydrogen not easily exchangeable (Schimmelmann et al., 2006), the δ²H$_{wax}$ is frequently

85   used in paleo-climate studies to track the variability of the ^{2}H/^{1}H ratio of meteoric water

86   (δ²H$_p$), as recently reviewed by Sachse et al. (2012). The 'altitude effect', described by

87   Dansgaard (1964), is one of the physical parameters impacting the δ²H$_p$ and it

88   corresponds to the progressive ²H-depletion of precipitation along altitudinal gradients

89   due to successive Rayleigh distillation equilibria as the air mass rises. This effect has

90   been observed in precipitation along several mountains across the world (Araguás-

91   Araguás et al., 2000) including 2 equatorial African mountains: Mt. Cameroon

92   (Cameroon; Gonfiantini et al., 2001) and Mt. Kilimanjaro (Tanzania; Zech et al., 2015).

93   The ability of δ²H$_{wax}$ to track this altitudinal effect was first shown at Mt. Gongga (China;

94   Jia et al., 2008). This relationship was further observed at several mountains in Asia,

95   Oceania and America (e.g. Luo et al., 2011; Ernst et al., 2013; Bai et al., 2015; Zhuang et

96   al., 2015).

97   Branched GDGTs represent another group of biomarkers increasingly used for

98   paleo-climate reconstructions in terrestrial archives (e.g. Peterse et al., 2011). These

99   membrane lipids (Suppl. Fig.) are ubiquitous in both terrestrial and aquatic environments

100   (Schouten et al., 2013) and are produced by yet unknown bacteria. In soils from across

101   the globe, the relative abundance of the different br GDGTs was shown to depend on

102   environmental parameters (Weijers et al., 2007), leading to the development of global

4

103   calibrations between br GDGT distribution and mean annual air temperature (MAAT)

104   and pH (Weijers et al., 2007; Peterse et al., 2012). These compounds can therefore be

105   used as paleo-thermometers. Soil-derived br GDGTs have been investigated along

106   several mountain transects (e.g.; Peterse et al., 2009; Ernst et al., 2013; Anderson et al.,

107   2014) with a high variability in temperature (as temperature decreases with altitude). In

108   the previously published papers, the related br GDGT-derived MAAT were found to (i)

109   be in agreement with local measured MAAT and (ii) relate with altitude (i.e. following

110   the natural temperature gradient), even though a high degree of scatter was observed for

111   some case studies (e.g. Mt. Gongga; Peterse et al., 2009).

112   The combination of δ^2H_{wax} and br GDGT provided promising results which

113   significantly expand their potential for (paleo) climate reconstruction. In modern soils,

114   they were found to both correlate with altitude along Mt. Gongga (China, Jia et al., 2008

115   and Peterse et al., 2009), Mt. Meghalaya (India, Ernst et al., 2013) and the Southern Alps

116   (New Zealand, Zhuang et al., 2015) implying that δ^2H_{wax} was recording the altitude effect

117   in δ^2H_p and br GDGTs the natural temperature gradient. In geological archives, the

118   approach has been employed to reconstruct the early Eocene elevation and climatic

119   history of the Sierra Nevada (Hren et al., 2010). It was deduced from the analysis of

120   δ^2H_{wax} from fossil leaves and br GDGTs from the sediment matrix that, during the

121   Eocene Climatic Optimum, Sierra Nevada elevation was high (> 2 km) with warmer air

122   temperature than today. In East Africa, however, altitudinal transects from the southern

123   slope of Mt. Kilimanjaro (Tanzania) was investigated by several groups (Sinninghe

124   Damsté et al., 2008; Peterse et al., 2009; Zech et al., 2015), resulting in inconsistent

125   results. While estimated air temperatures derived from the analysis of br GDGTs were

5

126   consistent with the observational temperature data (Sinninghe Damsté et al., 2008), no

127   clear altitudinal trend was observed for δ^2H_{wax} (Peterse et al., 2009; Zech et al., 2015).

128   This prompts the question regarding the relative importance of site (mountain)-related

129   and regional (East African)-related controls on the link between altitude and soil δ^2H_{wax}

130   record.

131   In the present study, δ^2H_{wax} and br GDGTs were analysed in 60 surface soils

132   along 2 East African mountains – Mt. Rungwe (n=40; Southwest Tanzania; Fig. 1) and

133   Mt. Kenya (n=20; Central Kenya; Fig. 1) – to further test their joint applicability as

134   (paleo) environmental proxies in this climatically sensitive area. Our results were then

135   combined with previously published data for 2 additional East African mountains (Mt.

136   Rwenzori, Uganda, Loomis et al., 2011; Mt. Kilimanjaro, Tanzania, Peterse et al., 2009,

137   Sinninghe Damsté et al., 2008 and Zech et al., 2015) to potentially generate regional

138   calibrations of δ^2H_{wax} variations with elevation and br GDGT variations with

139   temperature. This could improve the precision/quality of regional scale (paleo) elevation

140   and (paleo) temperature reconstructions in comparison with global calibrations. The

141   ultimate goal of this work is to introduce improved tools for terrestrially-based paleo-

142   climatic reconstructions in East Africa that take into account not only temperature but

143   also altitude changes, and which could then be used to reconstruct the evolution of

144   topography and climate dynamics over geological time in the EARS.

145

146

6

147   **2. Materials and Methods**

148

149   2.1. Study sites

150   Br GDGTs and *n*-alkanes were analysed in 40 surface soils collected between 500

151   and 2800 m along the gentle then steep slope of Mt. Rungwe in 2012 and 2014, and in 20

152   samples collected between 1900 and 3300 m along the steady gentle slope of Mt. Kenya

153   in 2013 (Table 1). About 50-60 g of soil were collected in the A horizon (0-5 cm) and

154   kept at room temperature before shipping to France by plane.

155   Mt. Rungwe is located in the Southwest of Tanzania (9° S, 33° E; Fig. 1) and

156   experiences a typical tropical climate, with alternations between a hot and humid (from

157   November to May) season and a colder and drier season (from June to October;

158   Delalande et al., 2008). Natural vegetation along the altitudinal transect belongs to the

159   Zambezian Miombo-type woodland at low altitude and Afromontane vegetation at higher

160   altitude (e.g. Vincens et al., 2003). Agriculture – including banana, rice, cocoa, tea,

161   coffee, maize cultivations – is practiced up to 1500 m leading to partial deforestation of

162   the mountain slopes (Williamson et al., 2014). MAAT was continuously measured with

163   temperature loggers (weather station, DAVIS, Instruments, Hayward, CA, USA) at 540

164   m, 920 m and 1720 m and varied from 25.6 °C at 540 m to 22.6 °C at 920 m and 16.9 °C

165   at 1720 m, leading to a temperature gradient of 0.7 °C/100 m.

166   Mt. Kenya is the highest mountain in Kenya (5199 m.a.s.l.) and is located on the

167   equator (0° S 37° E; Fig. 1). The twice-yearly passage of the Intertropical Convergence

168   Zone (ITCZ) leads to a bimodal rainfall pattern characterized by the onset and duration of

169   the long rains (March to May) and short rains (October to November), the other months

170   experiencing a drier climate (Camberlin et al., 2014). Present day vegetation is marked by

171   five distinguishable altitudinal zones, (Bremond et al., 2008; Hamilton, 1982) from the

172   mountain forest belt at its base (1960–2500 m.a.s.l.) to Afroalpine at its top (3400–

173   4200 m.a.s.l.), with Bamboo and Ericaceous zones in between. Based on meteorological

174   data from weather stations along Mt. Kenya and in Central Kenya (Camberlin et al.,

175   2014; Kenya Meteorological Department, 1984; Kenya Meteorological Department;

176   Smith, 1993), temperature lapse rate along Mount Kenya was determined as 0.63 °C/100

177   m.

178

179   2.2. Sample preparation

180   Samples were frozen and freeze-dried at their arrival in Paris (France) and then

181   kept at -18 °C prior further treatment. Sample preparation was identical to that detailed

182   by Coffinet et al. (2014). Briefly, soils were extracted (3×5 min) with dichloromethane

183   (DCM): methanol (MeOH) (9:1, v:v) using an accelerated solvent extractor (ASE 100 –

184   Dionex; 100°C, 10×10^6 Pa). The extract was separated into 2 fractions through a 2 cm

185   diam. column of Al_2O_3 (activated overnight at 150 °C) using heptane:DCM (9:1, v:v) and

186   DCM:MeOH (1:1, v:v) respectively. The 2 fractions were then rotary evaporated, re-

187   dissolved in 1 ml heptane and centrifuged using an Eppendorf Mini Spin centrifuge (1

188   min, 7000 rpm) prior to further analysis.

189

190   2.3. n-Alkane analysis

191   n-Alkanes were analysed at UPMC, Paris, France by gas chromatography coupled

192   to a mass spectrometer (GC-MS) using an Agilent Network 6890 GC System coupled

193   with a 5973 Mass Selective Detector, with electron impact at 70eV. 1 µl was injected and

8

194   the separation was achieved using a Restek RXI-5 Sil MS silica capillary column (30 m ×

195   0.25 mm i.d., 0.50 µm film thickness) with He as the carrier gas at 1 ml/min flow rate.

196   The GC oven initial temperature was set to 50 °C and then increased to 320 °C at a 4

197   °C/min. Samples were injected in splitless mode and the injector temperature was 280 °C.

198   n-Alkane hydrogen isotopic composition was measured at Newcastle University,

199   UK using a Delta V+ isotope-ratio mass spectrometer (IRMS, ThermoFisher) connected

200   to a GC Ultra Trace (ThermoFisher), a Finnigan GC Combustion III (ThermoFisher) and

201   a high temperature conversion (HTC) system set up at 1400 °C. The GC oven initial

202   temperature was set to 50 °C and then increased to 250 °C at 15 °C/min and from 250 °C

203   to 320 °C at 5 °C/min. The GC oven was held at 320 °C for 15 min. Every sample was

204   analysed in duplicate and the ^{2}H/^{1}H ratio was reported on the VSMOW (Vienna standard

205   mean ocean water) scale to determine compound specific $\delta^2 H_{Cn}$ (‰). The H_3 factor was

206   measured daily and varied between 2.48 and 2.61 during the course of analysis.

207   Sample n-alkane δ^2H values were corrected individually using an n-alkane standard (n-

208   C16 to n-C30; mix A5) and 5α-androstane standard (A. Schimmelmann, Indiana

209   University), run at the beginning and at the end of each sample sequence. Standard error

210   of the measurements of the long chain n-alkanes (C_{25}-C_{31}) from this standard mix ranged

211   between 0.3‰ and 1.1‰.

212

213   2.4. Br GDGT analysis

214   Br GDGT analysis was performed at UPMC, Paris, France by high pressure liquid

215   chromatography coupled to a mass spectrometer with an atmospheric pressure chemical

216   ionization source (HPLC-APCI-MS). Samples from Mt. Rungwe collected in 2014 were

9

217 analysed with a Shimadzu LCMS-2020, as described by Coffinet et al. (2015), whereas

218 samples from Mt. Kenya and those from Mt. Rungwe collected in 2012 were analysed

219 with an Agilent 1100 series HPLC instrument equipped with an automatic injector and

220 coupled to a PE Sciex API 3000 mass spectrometer, using a procedure described by

221 Coffinet et al. (2014). Similar chromatographic conditions were used on the 2 machines

222 and samples from Coffinet et al. (2014) were re-run with the Shimadzu LCMS-2020 to

223 assess the method reproducibility between the 2 LCMS apparatus (mean errors: 0.03 for

224 MBT, 0.05 for CBT and 0.28 °C for MAAT).

225   Semi-quantification of br GDGTs was performed by comparing the integrated

226 signal of the respective compound with the signal of a C_{46} synthesised internal standard

227 (Huguet et al., 2006) assuming their response factors to be identical.

228   The MBT' (methylation index of branched tetraethers; eq. 1; Peterse et al., 2012)

229 and CBT (cyclisation ratio of branched tetraethers; eq. 2; Weijers et al., 2007) indices

230 were determined from the following equations:

231 $$\text{MBT'} = \frac{[\text{Ia} + \text{Ib} + \text{Ic}]}{[\text{IIIa}] + [\text{IIa} + \text{IIb} + \text{IIc}] + [\text{Ia} + \text{Ib} + \text{Ic}]} \quad (1)$$

232 $$\text{CBT} = -\log\left(\frac{[\text{IIb}] + [\text{Ib}]}{[\text{IIa}] + [\text{Ia}]}\right) \quad (2)$$

233 Roman numerals refer to the structures in the Supplementary Figure.

234 Based on triplicate injections, the maximal analytical error for the different indices was:

235 0.09 for MBT' and 0.03 for CBT.

236   MAAT was estimated from the global soil calibration developed by Peterse et al.,

237   (2012; Eq. 3):

238          $MAAT = 0.81 - 5.67 \times CBT + 31.0 \times MBT'$ (3)

239

240   2.5. Estimation of the H isotopic composition of precipitation

241   To characterize the H isotope composition of precipitation (δ^2H_p) at the studied

242   sites, results from previous publications were gathered (Rieti-Shati et al., 2010; Nivet et

243   al., 2015; Zech et al., 2015). Due to the limited number of instrumental data, δ^2H_p was

244   also estimated with the Online Isotopes in Precipitation Calculator (OIPC; Bowen, 2016;

245   Bowen and Revenaugh, 2003). The OIPC model was developed to allow point estimation

246   of δ^2H_p. It is based on a spatial interpolation from the 340 Global Network for Isotope in

247   Precipitation (GNIP) station database. This interpolation includes the latitude and altitude

248   effects on the isotopic composition of precipitation but in some regions, including East

249   Africa, it is limited by additional sources of uncertainty. In East Africa, the major source

250   of uncertainty is the small number of GNIP stations which lowers the dataset resolution

251   (Bowen and Revenaugh, 2003; West et al., 2004) while the δ^2H_p variability is there

252   especially high (due to the intertropical context and the orographic complexity). In

253   addition, Bowen and Wilkinson (2002) pointed out 2 high altitude stations (Addis-Abeba

254   and Entebbe) where the measured isotopic composition of precipitation was anomalously

255   enriched in heavy isotopes, leading to an increased uncertainty in the prediction of δ^2H_p

256   in this region. For the estimations along the 3 studied mountains, the 95% confidence

257   level of the model varied from 3-4‰ at low altitudes to 6‰ at higher altitudes.

11

258   **3. Results**

259

260   3.1. δ^2Hp and δ^2Hwax along the altitudinal transects at Mt. Kenya and Mt. Rungwe

261   The δ^2H$_p$ values along Mts. Kenya, Rungwe and Kilimanjaro obtained using the

262   OIPC (the Online Isotopes in Precipitation Calculator; Bowen, 2016; Bowen and

263   Revenaugh, 2003; Fig. 2) span from -42‰ at 3270 m.a.s.l. to -23‰ at 1900 m.a.s.l. along

264   Mt. Kenya and from -49‰ at 2800 m.a.s.l. to -16‰ at 520 m.a.s.l. along Mt. Rungwe and

265   from -45‰ at 3245 m.a.s.l. to -23‰ at 1727 m.a.s.l along Mt. Kilimanjaro.

266   *n*-Alkanes were analysed in 20 soil samples collected between 1900 to 3160 m

267   along Mt. Kenya and in 40 soil samples collected between 500 and 2800 m along Mt.

268   Rungwe. The distribution parameters of these compounds (chain length range, C_n range;

269   average chain length, ACL; carbon preference index, CPI; cf. Supplementary Table 1) do

270   not show any statistically relevant correlation with altitude. Along the two transects, long

271   chain *n*-alkanes with odd-over-even predominance were the most abundant, as reflected

272   by overall high ACL (28 ± 2; Suppl. Table 1) and CPI values (between 3 and 18; Suppl.

273   Table 1). These results indicate that *n*-alkanes present in the soils originate predominantly

274   from higher plants. The δ^2H values are comprised between -109‰ and -177‰ (mean -

275   143‰) at Mt. Rungwe, and between -116‰ and -167‰ at Mt. Kenya (mean -141‰;

276   Suppl. Table 1). The weighted mean δ^2H$_{wax}$ of the long chain *n*-alkanes (C_{27}, C_{29}, C_{31})

277   varied between -166‰ and -125‰ (Table 1) along Mt. Rungwe and between -158‰ and

278   -119‰ along the slope at Mt. Kenya.

279

280

281

12

282　3.2. Br GDGT-derived mean annual air temperature (MAAT) along the altitudinal

283　transects at Mts. Rungwe and Kenya

284　　　　Br GDGTs were analysed along Mt. Kenya in the same soil samples as those

285　analysed for *n*-alkanes (n=20). Br GDGT proxies and corresponding temperature

286　estimates were previously determined in 20 surface soils collected at Mt. Rungwe in 2012

287　(Coffinet et al., 2014). This dataset was extended in the present study by the analysis of

288　br GDGTs in 16 additional soil samples (same sample set as for the *n*-alkane analysis

289　except 3 of them which were not analysed, see details in Table 1) collected along Mt.

290　Rungwe. The distribution of br GDGTs was similar in soils collected in 2012 and 2014,

291　as shown by the comparable ranges of MBT' and CBT values in these samples (cf. Suppl.

292　Table 2).

293　　　　Br GDGT-derived MAATs were estimated using the global soil calibration

294　(Peterse et al., 2012) and varied from 9.3 °C at 3270 m.a.s.l. to 16.9 °C at 1900 m.a.s.l.

295　along Mt. Kenya and from 12.2 °C at 2055 m.a.s.l. to 22.5 °C at 529 m.a.s.l. (Table 1).

296

297　**4. Discussion**

298

299　4.1. Variation of δ²H of *n*-alkanes in East Africa

300　　　　In East Africa, the altitude effect on the hydrogen isotopic ratio of precipitation

301　(δ^2H_p) was reported along Mt. Kilimanjaro above 2000 m.a.s.l. (1.4‰/100 m) while it

302　tends to be much weaker at lower altitudes (Zech et al., 2015 and Fig. 2). As Gonfiantini

303　et al. (2001) observed at Mt. Cameroon (Cameroon), the altitudinal gradient in the δ^2H_p

304　seems to increase with altitude. Along Mt. Rungwe, the establishment of a long term

305 monitoring of the isotopic composition of precipitation is ongoing (Nivet et al., 2015).

306 Preliminary data indicate values ranging from -16.9‰ at 1720 m.a.s.l. to -12.9‰ at 920

307 m.a.s.l. and -11.3‰ at 540 m.a.s.l. (Fig. 2) but more data are needed at higher altitudes to

308 compare with Mts. Kilimanjaro and Cameroon trends. Along Mt. Kenya, Rieti-Shati et al.

309 (2000) suggested the altitude effect to be absent based on precipitation events collected

310 between 3000 and 4000 m.a.s.l. and groundwater collection above 4500 m.a.s.l. However

311 this assumption is based on a very limited dataset from high altitude sampling sites on the

312 western side of the mountain whereas sampling for the present study was performed on

313 the North-East slope of Mt. Kenya. Long-term monitoring of precipitation along a wide

314 elevation range of this slope side at Mt. Kenya is needed to precisely assess the variation

315 of its isotopic composition.

316   Because of this limited number of measured isotopic values of precipitation along

317 the studied mountains, δ^2H_p had to be estimated using the OIPC (the Online Isotopes in

318 Precipitation Calculator; Bowen, 2016; Bowen and Revenaugh, 2003; Fig. 2). A ^{2}H-

319 depletion lapse rate of 1.5 ‰/100 m was computed for Mts. Rungwe and Kenya and of

320 1.4‰/100 m for Mt. Kilimanjaro, similar to the one measured by Zech et al. (2015)

321 above 2000 m.a.s.l. (Fig. 2). Nevertheless, along the latter, the OIPC data were observed

322 to be shifted from the measured ones, particularly at higher altitudes, towards more

323 depleted values and to a higher extent than the 95% confidence level estimated by the

324 model (ca. 11‰ difference; Fig. 2). Such a shift was already observed and discussed in

325 Kenya by Soderberg et al. (2013) and is likely due to the low number of GNIP stations

326 whilst the rain composition exhibits a high spatial variability in the region. Therefore the

327 absolute values derived from the OIPC must be treated with caution. However, they

14

328　should depict the likely trend of δ^2H_p related to the altitude effect and allow comparison

329　between the three studied sites. Notably, the δ^2H_p varies from one mountain to another

330　(Fig. 2). At a given altitude, 870 m.a.s.l. for example, δ^2H_p equals -22‰, -12‰, -8‰

331　along Mts. Rungwe, Kilimanjaro and Kenya, respectively. More specifically, the more

332　northern the latitude, the more enriched the δ^2H_p. This illustrates that, in addition to

333　altitude, a latitudinal effect is also likely to impact the δ^2H_p distribution in East Africa, as

334　previously noted at the global scale by Dansgaard (1964). No calibration of δ^2H_p with

335　altitude could thus be deduced at the regional, East African, scale and the altitudinal

336　effect in δ^2H_p could only be tracked at the mountain scale. Consequently, in the

337　following, the ability of δ^2H of *n*-alkanes (δ^2H_{wax}) to track the altitudinal effect on δ^2H_p

338　was solely investigated at the mountain scale for each study site.

339　　　　The concentration-weighted mean values of δ^2H C_{27} – C_{31} alkanes (δ^2H_{wax}, Table

340　1) were plotted against altitude for Mt. Kenya and Mt. Rungwe (Fig. 3A-B). A

341　statistically significant, though scattered, ^2H-depletion trend was observed along Mt.

342　Kenya (-1.2‰/100 m; Fig. 3A; $p < 0.05$) close to the gradient observed for precipitation

343　along Mt. Kilimanjaro (-1.4‰/100 m, Fig. 2). This result indirectly suggests the

344　existence of an altitude effect in δ^2H_p along Mt. Kenya, unlike what was previously

345　reported by Rieti-Shati et al. (2000). The δ^2H_{wax} values along Mt. Kenya support the

346　hypothesis that *n*-alkanes are able to record the altitude effect in their $^2H/^1H$ ratio,

347　consistent with evidence from several other mountain systems in Asia (e.g. Jia et al.,

348　2008; Bai et al., 2015) and New Zealand (Zhuang et al., 2015). In contrast, no trend was

349　noticed at Mt. Rungwe (Fig. 3B, $p> 0.05$), as previously observed along Mt. Kilimanjaro

350　(Peterse et al., 2009; Zech et al., 2015).

351   For these two mountains (Rungwe and Kilimanjaro), we suggest that the altitude

352   effect observed in the precipitation may have been overprinted during the biosynthesis of

353   n-alkanes and/or their diagenetic reworking in the soil. As reviewed by Sachse et al.

354   (2012), lipid biosynthesis comprises several steps where $^2H/^1H$ fractionation can occur.

355   The magnitude of fractionation on the end-product δ^2H_{wax} signal is still poorly

356   constrained for most plant species. Notably, Sachse et al. (2012) highlighted several

357   parameters that could have a high impact on the δ^2H_{wax} fractionation, such as vegetation

358   changes, deposition processes and leaf physiology. Several studies pointed out large

359   variability in the leaf-derived δ^2H_{wax} of different species within a same site (e.g.

360   Chikaraishi and Naraoka, 2007; Pedentchouk et al., 2008). Thus, the important vegetation

361   changes with altitude documented along Mts. Kilimanjaro and Rungwe (Bremond et al.,

362   2008; Williamson et al., 2014) could have influenced the δ^2H_{wax} signal, leading to an

363   overprinting of the altitude effect on the δ^2H of the precipitation. Moreover, Zech et al.

364   (2015) postulated that along Mt. Kilimanjaro the altitudinal effect should be outcompeted

365   by the increasing evaporative ^2H-enrichment of the leaf water due to changes in humidity

366   with increasing altitude. The impact of these potential additional effects could be

367   enhanced in East Africa, where the altitude effects on δ^2H_p (Fig. 2) are in the lower range

368   of the gradients measured across the world (between -1 and -4‰/100 m, Araguás-

369   Araguás et al., 2000).

370   The results from this study highlight the complexity of the H isotopic signal

371   recorded in n-alkanes from East African soils. The altitude effect on δ^2H_p was recorded in

372   the δ^2H_{wax} signal at only one altitudinal transect (Mt. Kenya). This suggests that the use

373   of δ^2H_{wax} as a (paleo) elevation proxy might be site-dependent. This study also points to

16

374 the competitive impact of different hydroclimatic and biogeochemical factors on the soil

375 δ^2H_{wax} record. Unfortunately the lack of extensive environmental monitoring in these

376 remote locations prevented us from determining which of these factors are overprinting

377 the δ^2H_{wax} signal at the other two mountains. Notably, more instrmental data are needed

378 to improve the estimation of the δ^2H_p in East Africa. These observations probably also

379 hold for other mountainous regions across the world and should therefore be taken into

380 consideration in regional scale (paleo) elevation studies. The application of δ^2H_{wax} for

381 (paleo) elevation reconstructions must therefore be limited to the mountain scale and

382 should always be accompanied by detailed surveys of the environmental setting of the

383 study site.

384

385 4.2. East African regional br GDGT calibration

386   Linear altitudinal gradients of measured mean annual air temperatures (MAAT)

387 were observed along all the investigated East African mountains: 0.56 °C/100 m in Mt.

388 Kilimanjaro (Tanzania, Sinninghe Damsté et al., 2008),, 0.53 °C/100 m in Mt. Rwenzori

389 (Uganda, Loomis et al., 2011), 0.73 °C/100 m in Mt. Rungwe (Tanzania, Coffinet et al.,

390 2014, Williamson et al., 2014) and 0.63 °C/100 m in Mt. Kenya (Kenya, Camberlin et al.,

391 2014; Kenya Meteorological Department, 1984; Kenya Meteorological Department;

392 Smith, 1993).   The goal of this study was to investigate whether it is possible to establish

393 a regional East African framework for the use of soil derived-br GDGTs as a paleo-

394 thermometer. Thus, the measured MAAT data from all the local East African transects

395 mentioned above were combined to calculate a regional temperature lapse rate (Fig. 4).

396 This rate, determined as 0.65 °C/100 m, with 97% of the MAAT variance being

17

397   explained by altitudinal variations (Fig. 4), is similar to the one commonly used in low

398   precision studies (Rolland, 2003; Grab, 2013 and references therein) and will allow us to

399   assess the effect of temperature changes on br GDGT distribution at the regional scale.

400   In addition to Mts. Kenya and Rungwe investigated in the present study, br

401   GDGT distribution was previously investigated along two additional East African

402   mountains, Mt. Rwenzori (Uganda; Loomis et al., 2011) and Mt. Kilimanjaro (Tanzania,

403   Sinninghe Damsté et al., 2008). Br GDGT-derived MAATs were estimated using the

404   global soil calibration (Peterse et al., 2012; Weijers et al., 2007) and were found to

405   successfully record the decrease in MAAT with altitude along the slopes of these two

406   previously studied mountains. However, the soils sampled at the highest elevations in Mt.

407   Rwenzori exhibited a significant cold bias (Loomis et al., 2011). The authors suggested

408   that the water saturation of these soils may additionally impact the br GDGT distribution.

409   An impact of extreme soil water content (either aridity or saturation) on br GDGT

410   distribution and corresponding temperature estimates has indeed been reported in several

411   publications (e.g. Huguet et al., 2010 Dirghangi et al., 2013; Menges et al. 2014; Dang et

412   al., 2016).

413   Br GDGT-derived MAATs calculated using the soil calibration by Peterse et al.

414   (2012) were also shown to decrease linearly with altitude along Mts. Rungwe and Kenya

415   ($R^2 = 0.79$ and 0.66 respectively; figures not shown). Combined together, these four

416   studies highlight the robustness of br GDGTs as a paleo-temperature proxy, at least for

417   East Africa (MAAT lapse-rate = 0.4 °C/100 m, $R^2 = 0.63$; Fig. 5C). Despite this positive

418   assessment, the application of the global soil calibration still leads to a substantial

18

419 uncertainty in temperature reconstruction (Root Mean Square Error (RMSE) = 4.2 °C,

420 Peterse et al., 2012; R² = 0.56, Fig. 5A).

421   Combination of the new and previously published (Sinninghe Damsté et al., 2008;

422 Loomis et al., 2011; Coffinet et al., 2014) data from East Africa, leads to a br GDGT

423 dataset from in total 105 soils. Because of the potential additional impact of water

424 saturation on brGDGT distribution and thus associated temperature estimates, the high

425 elevation samples from Loomis et al. (2011) were not used in this dataset. Based on this

426 integrated sample set, a least square multiple linear regression was performed between br

427 GDGT distribution (MBT' and CBT indices) and the available MAAT for the four sites

428 (Mt. Kenya, Rwenzori, Kilimanjaro and Rungwe). The following equation was obtained:

429 $MAAT = -8.76 \times CBT + 24.24 \times MBT' + 9.60$ (R² = 0.77, RMSE = 2.4 °C) (4)

430   This regional soil calibration (Fig. 5B) strongly improves both the R² and RMSE

431 of br GDGT-reconstructed MAAT over the global soil calibration derived from globally

432 distributed soils (Fig. 5A, Peterse et al., 2012). The new East African calibration

433 produces robust quantitative temperatures from br GDGT distributions in soils as it takes

434 into account the regional specificities in soil water content, soil type, biome type, all of

435 which that could potentially impact br GDGT abundance and distribution (e.g. Dirghangi

436 et al., 2013; Menges et al., 2014). This highlights the necessity for regional

437 determinations of the relationship between temperature and br GDGT distribution in

438 order to improve past-temperature estimates. But it also points to the question of defining

439 coherent regions over the globe with a relevant scale.

440   The East African soil calibration developed in this study was applied to the

441 MAAT reconstruction in modern soils along all four altitudinal transects (Fig. 5D). The

19

442 resultant br GDGT-derived MAAT lapse rate (0.52 °C/100 m; Fig. 5D) is closer to the

443 measured one (0.65 °C/100 m; Fig. 5D) than when using the global soil calibration (0.41

444 °C/100 m; 5C), but still underestimates the actual lapse rate by ca. 20 %. This points to

445 the unsuitability of using br GDGTs alone to reconstruct past elevation changes.

446 Independently of that, the correlation between MAAT estimates and altitude is higher

447 when using the new regional soil calibration ($R^2 = 0.80$; Fig. 5D) than the global one (R^2

448 = 0.63; Fig. 5C), and closer to the correlation found between instrumental MAAT and

449 altitude ($R^2 = 0.97$; Fig. 4).. Therefore, the consistency and increase in quality of this new

450 regional calibration for temperature reconstruction calls for its wider application in

451 paleosol-based paleo-climatic reconstructions in East Africa. So far, in this region, br

452 GDGT-derived proxies have only been used in lacustrine sedimentary records (e.g.

453 Tierney et al., 2010; Sinninghe Damsté et al., 2012). This regional but valuable climatic

454 information can also be deduced from paleosol sequences (e.g. Hatté et al., 2001; Gocke

455 et al., 2014), which are abundant in East Africa due to the high rate of volcanic activity

456 (e.g. in the Rungwe volcanic province, Fontijn et al., 2010). First applications of br

457 GDGTs in such soil settings from across the world have revealed promising results (e.g.

458 Peterse et al., 2011; Zech et al., 2012).

459

460   **5. Conclusions**

461

462   δ^2H_{wax} and br GDGT distributions were determined in 60 surface soils collected

463 along altitudinal transects of two East African mountains (Mt. Rungwe in Tanzania and

464 Mt. Kenya in Kenya). The obtained values were combined with data from altitudinal

465 gradients of previous studies in the region to assess the applicability of integrated δ^2H_{wax}

20

466   and br GDGTs data sets as coupled paleo-topography and paleo-temperature proxies,

467   respectively, in East Africa. Variations in δ^2H_{wax} do not systematically document

468   altitudinal changes, with only one out of the three investigated mountains showing a

469   positive relationship – even though the altitude effect was present in the δ^2H of

470   precipitation. At the regional (East African) scale, coupling of estimated and observed

471   δ^2H_p data highlights their spatial heterogeneity. The use of δ^2H_{wax} as a paleo-elevation

472   proxy must therefore be restricted to site (mountain)-specific studies. In contrast, br

473   GDGT-derived MAAT reliably track measured MAAT gradients along the four studied

474   mountains (Mts Rungwe, Kenya, Kilimanjaro and Rwenzori). The large dataset of both

475   measured and br GDGT-derived MAAT in the study area enabled to establish a new

476   regional East African soil calibration between br GDGT distribution and MAAT. This

477   new calibration improves the accuracy of MAAT reconstruction for the studied region, in

478   comparison to other global soil calibrations, and highlights the potential of br GDGTs as

479   paleo-thermometers in recent and ancient East African soils.

480

481   **Acknowledgements**

21

493

References:

495 Anderson V.J., Shanahan T.M., Saylor J.E., Horton B.K., Mora A.R. (2014). Sources of
496   local and regional variability in the MBT′/CBT paleotemperature proxy: Insights
497   from a modern elevation transect across the Eastern Cordillera of Colombia. *Org.*
498   *Geochem.* **69**, 42–51.
499 Araguás-Araguás L., Froehlich K., Rozanski K. (2000). Deuterium and oxygen-18
500   isotope composition of precipitation and atmospheric moisture. *Hydrol. Process.*
501   **14**, 1341–1355.
502 Bai Y., Fang X., Jia G., Sun J., Wen R., Ye Y. (2015). Different altitude effect of leaf
503   wax n-alkane δD values in surface soils along two vapor transport pathways,
504   southeastern Tibetan Plateau. *Geochim. Cosmochim. Acta* **170**, 94–107.
505 Bremond L., Alexandre A., Wooller M.J., Hély C., Williamson D., Schäfer P.A., Majule
506   A., Guiot J. (2008). Phytolith indices as proxies of grass subfamilies on East
507   African tropical mountains. *Global Planet. Change* **61**, 209–224.
508 Bowen G. J. (2016) The Online Isotopes in Precipitation Calculator, version 2.2.
509   http://www.waterisotopes.org.
510 Bowen, G. J., and Wilkinson B. (2002), Spatial distribution of δ^{18}O in meteoric
511   precipitation, *Geology* **30**, 315–318.
512 Bowen G.J. and Revenaugh J. (2003). Interpolating the isotopic composition of modern
513   meteoric precipitation. *Water Resour. Res.* **39**, 1299.
514 Camberlin P., Boyard-Micheau J., Philippon N., Baron C., Leclerc C., Mwongera C.
515   (2014). Climatic gradients along the windward slopes of Mount Kenya and their
516   implication for crop risks. Part 1: climate variability. *Int. J. Climatol.* **34**, 2136–
517   2152.
518 Chikaraishi Y. and Naraoka H. (2007). δ^{13}C and δD relationships among three n-alkyl
519   compound classes (n-alkanoic acid, n-alkane and n-alkanol) of terrestrial higher
520   plants. *Org. Geochem.* **38**, 198–215.
521 Coffinet, S., Huguet, A., Williamson, D., Fosse, C., Derenne, S., 2014. Potential of
522   GDGTs as a temperature proxy along an altitudinal transect at Mount Rungwe
523   (Tanzania). *Org. Geochem.* **68**, 82–89.
524 Coffinet S., Huguet A., Williamson D., Bergonzini L., Anquetil C., Majule A., Derenne
525   S. (2015). Occurrence and distribution of glycerol dialkanol diethers and glycerol

526   dialkyl glycerol tetraethers in a peat core from SW Tanzania. *Org. Geochem.* **83–**
527   **84**, 170–177.
528 Dang X., Yang H., Naafs D.A., Pancost R.D., Xie S., 2016. Evidence of moisture control
529   on the methylation of branched glycerol dialkyl glycerol tetraethers in semi-arid
530   and arid soils. *Geochim. Cosmochim. Acta* **189**, 24-36.
531 Dansgaard W. (1964). Stable isotopes in precipitation. *Tellus XVI* **4**, 436-468.
532 Delalande M., Bergonzini L., Massault M. (2008). Mbaka lakes isotopic (^{18}O and ^{2}H) and
533   water balances: discussion on the used atmospheric moisture compositions. *Isot*
534   *Environ Healt. S.* **44**, 71–82.
535 Dirghangi S.S., Pagani M., Hren M.T., Tipple B.J. (2013). Distribution of glycerol
536   dialkyl glycerol tetraethers in soils from two environmental transects in the USA.
537   *Org. Geochem.* **59**, 49–60.
538 Eglinton G. and Hamilton R.J. (1967). Leaf epicuticular waxes. *Science, New Series* **156**,
539   1322–1335.
540 Eglinton T.I. and Eglinton G. (2008). Molecular proxies for paleoclimatology. *Earth*
541   *Planet. Sc. Lett.* **275**, 1–16.
542 Ernst N., Peterse F., Breitenbach S.F.M., Syiemlieh H.J., Eglinton T.I. (2013).
543   Biomarkers record environmental changes along an altitudinal transect in the
544   wettest place on Earth. *Org. Geochem.* **60**, 93-99.
545 Fontijn K., Ernst G.G.J., Elburg M.A., Williamson D., Abdallah E., Kwelwa S., Mbede
546   E., Jacobs P. (2010). Holocene explosive eruptions in the Rungwe Volcanic
547   Province, Tanzania. *J. Volcanol. Geoth. Res.* **196**, 91–110.
548 Gocke M., Hambach U., Eckmeier E., Schwark L., Zöller L., Fuchs M., Löscher M.,
549   Wiesenberg G.L.B. (2014). Introducing an improved multi-proxy approach for
550   paleoenvironmental reconstruction of loess–paleosol archives applied on the Late
551   Pleistocene Nussloch sequence (SW Germany). *Palaeogeogr. Palaeoclimatol.*
552   *Palaeoecol.* **410**, 300–315.
553 Gonfiantini R., Roche M.-A., Olivry J.-C., Fontes J.-C., Zuppi G.M. (2001). The altitude
554   effect on the isotopic composition of tropical rains. *Chem. Geol.* **181**, 147–167.
555 Grab, S.W. (2013). Fine-scale variations of near-surface-temperature lapse rates in the
556   high Drakensberg escarpment, South Africa: environmental implications. *Arct.*
557   *Antarct. Alp. Res.* **45**, 500–514.
558 Hatté C., Antoine P., Fontugne M., Lang A., Rousseau D.-D., Zöller L. (2001). δ^{13}C of
559   Loess Organic Matter as a Potential Proxy for Paleoprecipitation. *Quaternary Res.*
560   **55**, 33–38.
561 Hijmans R.J., Cameron S.E., Parra J.L., Jones P.G., Jarvis A. (2005). Very high
562   resolution interpolated climate surfaces for global land areas. *Int. J. Climatol.* **25**,
563   1965–1978.
564 Hren M.T., Pagani M., Erwin D.M., Brandon M. (2010). Biomarker reconstruction of the
565   early Eocene paleotopography and paleoclimate of the northern Sierra Nevada.
566   *Geology* **38**, 7–10.
567 Huguet C., Hopmans E.C., Febo-Ayala W., Thompson D.H. Sinninghe Damsté J.S.,
568   Schouten S. (2006). An improved method to determine the absolute abundance of
569   glycerol dibiphytanyl glycerol tetraether lipids. *Org. Geochem.* **37**, 1036–1041.

570 Huguet, A., Fosse, C., Laggoun-Défarge, F., Toussaint, M.-L., Derenne, S. (2010).
571   Occurrence and distribution of glycerol dialkyl glycerol tetraethers in a French
572   peat bog. *Org. Geochem.* **41**, 559–572.
573 Jia G., Wei K., Chen F., Peng P. (2008). Soil n-alkane δD vs. altitude gradients along
574   Mount Gongga, China. *Geochim. Cosmochim. Acta* **72**, 5165–5174.
575 Kenya Meteorological Department, 1984: Climatological statistics for Kenya. KMD,
576   Nairobi, 87 p.
577 Loomis S.E., Russell J.M., Sinninghe Damsté J.S. (2011). Distributions of branched
578   GDGTs in soils and lake sediments from western Uganda: Implications for a
579   lacustrine paleothermometer. *Org. Geochem.* **42**, 739–751.
580 Luo P., Peng P. 'an, Gleixner G., Zheng Z., Pang Z., Ding Z. (2011). Empirical
581   relationship between leaf wax n-alkane δD and altitude in the Wuyi, Shennongjia
582   and Tianshan Mountains, China: Implications for paleoaltimetry. *Earth Planet.*
583   *Sc. Lett.* **301**, 285–296.
584 Macgregor D. (2015). History of the development of the East African Rift System: A
585   series of interpreted maps through time. *J. Afr. Earth Sci.* **101**, 232–252.
586 Menges J., Huguet C., Alcañiz J.M., Fietz S., Sachse D., Rosell-Melé A. (2014).
587   Influence of water availability in the distributions of branched glycerol dialkyl
588   glycerol tetraether in soils of the Iberian Peninsula. *Biogeosciences* **11**, 2571–
589   2581.
590 Nivet, F., Bergonzini, L., Diemer, L., Mathé, P.-E., Kajula, S., Ngingo, P., Mwasomba,
591   A., Noret, A., Majule, A., Williamson, D. (2015). RESON: 3-year records of
592   rainfall isotopic composition from 3 stations of the Rungwe volcanic province
593   (SW Tanzania). Presented at *Tropical deserts and lakes through time,*
594   *Paleohydrology, Isotope geochemistry, Climate and Societies*, Aix-en-Provence
595   (France).
596 Pedentchouk N., Sumner W., Tipple B., Pagani M. (2008). δ^{13}C and δD compositions of
597   n-alkanes from modern angiosperms and conifers: An experimental set up in
598   central Washington State, USA. *Org. Geochem.* **39**, 1066–1071.
599 Peterse F., van der Meer M.T.J., Schouten S., Jia G., Ossebaar J., Blokker J., Sinninghe
600   Damsté J.S. (2009). Assessment of soil n-alkane delta D and branched tetraether
601   membrane lipid distributions as tools for paleoelevation reconstruction.
602   *Biogeosciences* **6**, 2799–2807.
603 Peterse F., Prins M.A., Beets C.J., Troelstra S.R., Zheng H., Gu Z., Schouten S.,
604   Sinninghe Damsté J.S. (2011). Decoupled warming and monsoon precipitation in
605   East Asia over the last deglaciation. *Earth Planet. Sc. Lett.* **301**, 256–264.
606 Peterse F., van der Meer J., Schouten S., Weijers J.W.H., Fierer N., Jackson R.B., Kim J.-
607   H., Sinninghe Damsté J.S. (2012). Revised calibration of the MBT–CBT
608   paleotemperature proxy based on branched tetraether membrane lipids in surface
609   soils. *Geochim. Cosmochim. Acta* **96**, 215–229.
610 Rieti-Shati M., Yam R., Karlen W, Shemesh A. (2000). Stable isotope composition of
611   tropical high-altitude fresh-waters on Mt. Kenya, Equatorial East Africa. *Chem*
612   *Geol* **166**, 341-350.
613 Rolland, C. (2003). Spatial and Seasonal Variations of Air Temperature Lapse Rates in
614   Alpine Regions. *J. Climate* **16**, 1032–1046.

615 Sachse D., Billault I., Bowen G.J., Chikaraishi Y., Dawson T.E., Feakins S.J., Freeman
616   K.H., Magill C.R., McInerney F.A., van der Meer M.T.J., Polissar P., Robins R.J.,
617   Sachs J.P., Schmidt H.-L., Sessions A.L., White J.W.C., West J.B., Kahmen A.
618   (2012). Molecular Paleohydrology: Interpreting the Hydrogen-Isotopic
619   Composition of Lipid Biomarkers from Photosynthesizing Organisms. *Annu. Rev.*
620   *Earth Pl. Sc.* **40**, 221–249.
621 Sauer P.E., Eglinton T.I., Hayes J.M., Schimmelmann A., Sessions A.L. (2001).
622   Compound-specific D/H ratios of lipid biomarkers from sediments as a proxy for
623   environmental and climatic conditions. *Geochim. Cosmochim. Acta* **65**, 213–222.
624 Schimmelmann A., Sessions A.L., Mastalerz M. (2006). Hydrogen Isotopic (D/H)
625   Composition of Organic Matter During Diagenesis and Thermal Maturation.
626   *Annu. Rev. Earth Pl. Sc.* **34**, 501–533.
627 Schouten S., Hopmans E.C., Sinninghe Damsté J.S. (2013). The organic geochemistry of
628   glycerol dialkyl glycerol tetraether lipids: A review. *Org. Geochem.* **54**, 19–61.
629 Sepulchre P., Ramstein G., Fluteau F., Schuster M., Tiercelin J.-J., Brunet M. (2006).
630   Tectonic Uplift and Eastern Africa Aridification. *Science, New Series* **313**, 1419–
631   1423.
632 Sinninghe Damsté J.S., Ossebaar J., Schouten S., Verschuren D. (2008). Altitudinal shifts
633   in the branched tetraether lipid distribution in soil from Mt. Kilimanjaro
634   (Tanzania): Implications for the MBT/CBT continental palaeothermometer. *Org.*
635   *Geochem.* **39**, 1072–1076.
636 Sinninghe Damsté J.S., Ossebaar J., Schouten S., Verschuren D. (2012). Distribution of
637   tetraether lipids in the 25-ka sedimentary record of Lake Challa: extracting
638   reliable TEX_{86} and MBT/CBT palaeotemperatures from an equatorial African
639   lake. *Quaternary Sci. Rev.* **50**, 43–54.
640 Soderberg K., Good S.P., O'Connor M., Wang L., Ryan K., Caylor K.K. (2013). Using
641   atmospheric trajectories to model the isotopic composition of rainfall in central
642   Kenya. *Ecosphere* **4**, 1–18.
643 Smith, M. (1993). CLIMWAT for CROPWAT: A climatic database for irrigation
644   planning and management (No. FAO IDP-49). FAO, Roma (Italia).
645   Agrometeorological Group.
646 Tierney J.E., Russell J.M., Eggermont H., Hopmans E.C., Verschuren D., Sinninghe
647   Damsté J.S. (2010). Environmental controls on branched tetraether lipid
648   distributions in tropical East African lake sediments. *Geochim. Cosmochim. Acta*
649   **74**, 4902–4918.
650 Verschuren D., Sinninghe Damsté J.S., Moernaut J., Kristen I., Blaauw M., Fagot M.,
651   Haug G.H., Geel B. van, Batist M.D., Barker P., Vuille M., Conley D.J., Olago
652   D.O., Milne I., Plessen B., Eggermont H., Wolff C., Hurrell E., Ossebaar J.,
653   Lyaruu A., Plicht J. van der, Cumming B.F., Brauer A., Rucina S.M., Russell
654   J.M., Keppens E., Hus J., Bradley R.S., Leng M., Mingram J., Nowaczyk N.R.
655   (2009). Half-precessional dynamics of monsoon rainfall near the East African
656   Equator. *Nature* **462**, 637–641.
657 Vincens A., Williamson D., Thevenon F., Taieb M., Buchet G., Decobert M., Thouveny
658   N. (2003). Pollen-based vegetation changes in southern Tanzania during the last
659   4200 years: climate change and/or human impact. *Palaeogeogr. Palaeoclimatol.*
660   *Palaeoecol.* **198**, 321–334.

661 Weijers J.W.H., Schouten S., van den Donker J.C., Hopmans E.C., Sinninghe Damsté
662   J.S. (2007). Environmental controls on bacterial tetraether membrane lipid
663   distribution in soils. *Geochim. Cosmochim. Acta* **71**, 703–713.
664 West, A.G., February, E.C., Bowen, G.J. (2014). Spatial analysis of hydrogen and oxygen
665   stable isotopes ("isoscapes") in ground water and tap water across South Africa. *J.*
666   *Geochem. Explor.* **145**, 213–222.
667 Williamson D., Majule A., Delalande M., Mwakisunga B., Mathé P.-E., Gwambene B.,
668   Bergonzini L. (2014). A potential feedback between landuse and climate in the
669   Rungwe tropical highland stresses a critical environmental research challenge.
670   *Curr. Opin. Environ. Sustain.* **6**, 116–122.
671 Zech M., Zech R., Rozanski K., Gleixner G., Zech W. (2015). Do n-alkane biomarkers in
672   soils/sediments reflect the δ2H isotopic composition of precipitation? A case
673   study from Mt. Kilimanjaro and implications for paleoaltimetry and paleoclimate
674   research. *Isot Environ Healt. S.* **51**, 508–524.
675 Zech R., Gao L., Tarozo R., Huang Y. (2012). Branched glycerol dialkyl glycerol
676   tetraethers in Pleistocene loess-paleosol sequences: Three case studies. *Org.*
677   *Geochem.* **53**, 38–44.
678 Zhuang G., Pagani M., Chamberlin C., Strong D., Vandergoes M. (2015). Altitudinal
679   shift in stable hydrogen isotopes and microbial tetraether distribution in soils from
680   the Southern Alps, NZ: Implications for paleoclimatology and paleoaltimetry.
681   *Org. Geochem.* **79**, 56–64.

Figure captions

682

683 **Fig. 1.** Map of East Africa. The different sites mentioned in this study are represented
684 with a star. A zoom-in is made for Mt. Kenya and Mt. Rungwe, the 2 sites specifically
685 investigated in this study, and altitudinal profiles of the corresponding transects are
686 shown.

687

688 **Fig. 2.** δ^2H_p estimations from the OIPC (the Online Isotopes in Precipitation Calculator;
689 Bowen, 2016; Bowen and Revenaugh, 2003) along Mt. Rungwe, Tanzania (red segment),
690 Mt. Kenya, Kenya (green segment) and Mt. Kilimanjaro, Tanzania (blue segment)
691 together with on field δ^2H_p measurements along Mt. Kilimanjaro (blue circles; Zech et
692 al., 2015) and Mt. Rungwe (red diamonds; Nivet et al. 2015). Note that the delimitations
693 of each segment corresponds to the altitudinal range of the sample set investigated in the
694 present study for each mount.

695

696 **Fig. 3.** δ^2H_{wax} values (A) along the altitudinal transects at Mt. Kenya, Kenya and (B)
697 along the altitudinal transect at Mt Rungwe, Tanzania.

698

699 **Fig. 4.** Measured mean annual air temperature (MAAT) along altitudinal gradients in
700 East Africa: Mt Rungwe (red diamonds; Coffinet et al., 2014); Mt. Kenya (green
701 triangles; Camberlin et al., 2014), Mt. Rwenzori (purple squares; Loomis et al., 2011),
702 Mt. Kilimanjaro (blue circles; Sinninghe Damsté et al., 2008)

703

704 **Fig. 5.** Comparison of the accuracy and precision of (A) the global soil MBT'/CBT
705 calibration (Peterse et al., 2012) and (B) the new East African regional MBT'/CBT
706 calibration developed in this study, the 1:1 line being represented in dashed grey as a
707 reference. Application of these 2 calibrations to reconstruct br GDGT-derived MAAT
708 variation with altitude in East Africa: (C) the global soil calibration (Peterse et al., 2012),
709 (D) the new East African soil calibration where the black solid line is the derived linear
710 regression obtained from br GDGT-derived MAAT and the dashed black line is the
711 measured MAAT altitudinal gradient (as obtained in Fig. 3). Colours correspond to each
712 mountain of the region: Mt Rungwe (red diamonds; Mt. Rungwe, this study and Coffinet
713 et al., 2014); Mt. Kenya (green triangles; this study), Mt. Rwenzori (purple squares;
714 Loomis et al., 2011), Mt. Kilimanjaro (blue circles; Sinninghe Damsté et al., 2008);

715

716

717 **Table 1.** Weighted average δ^2H of C_{27}, C_{29} and C_{31} n-alkanes (denoted δ^2H_{wax}) together
718 with br GDGT-derived mean annual air temperature (MAAT) from Peterse et al. (2012)
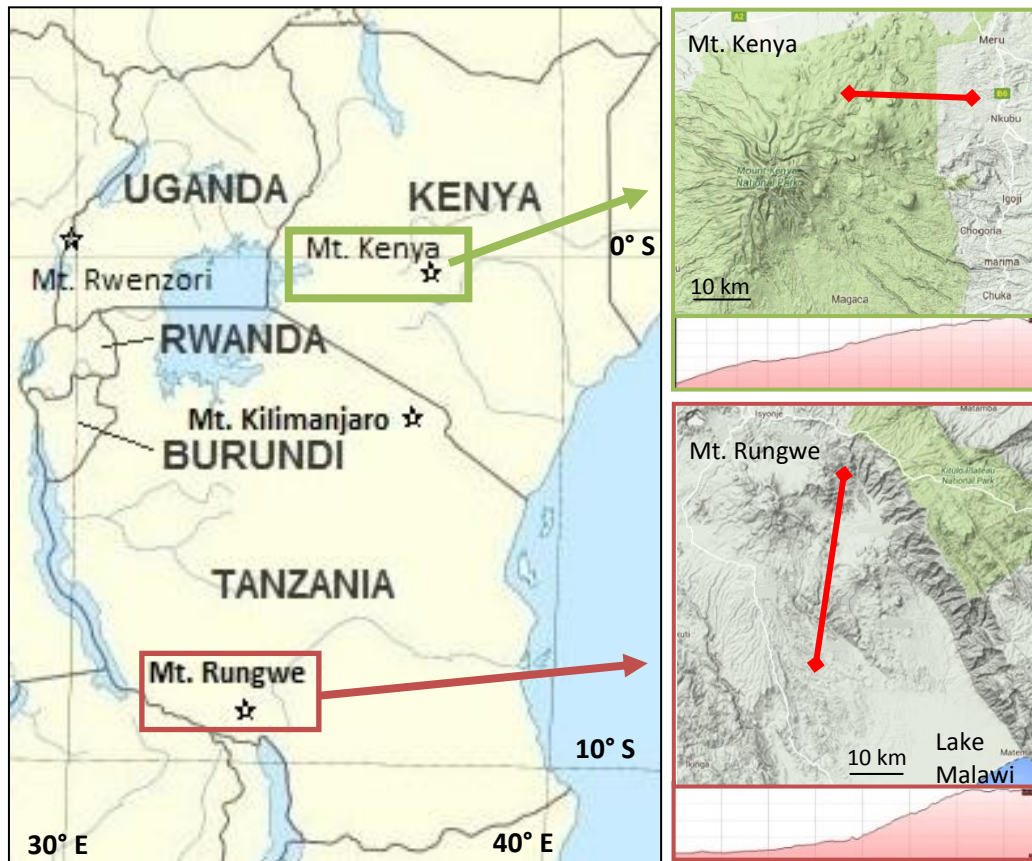719 calibration and from the regional calibration developed in this study.
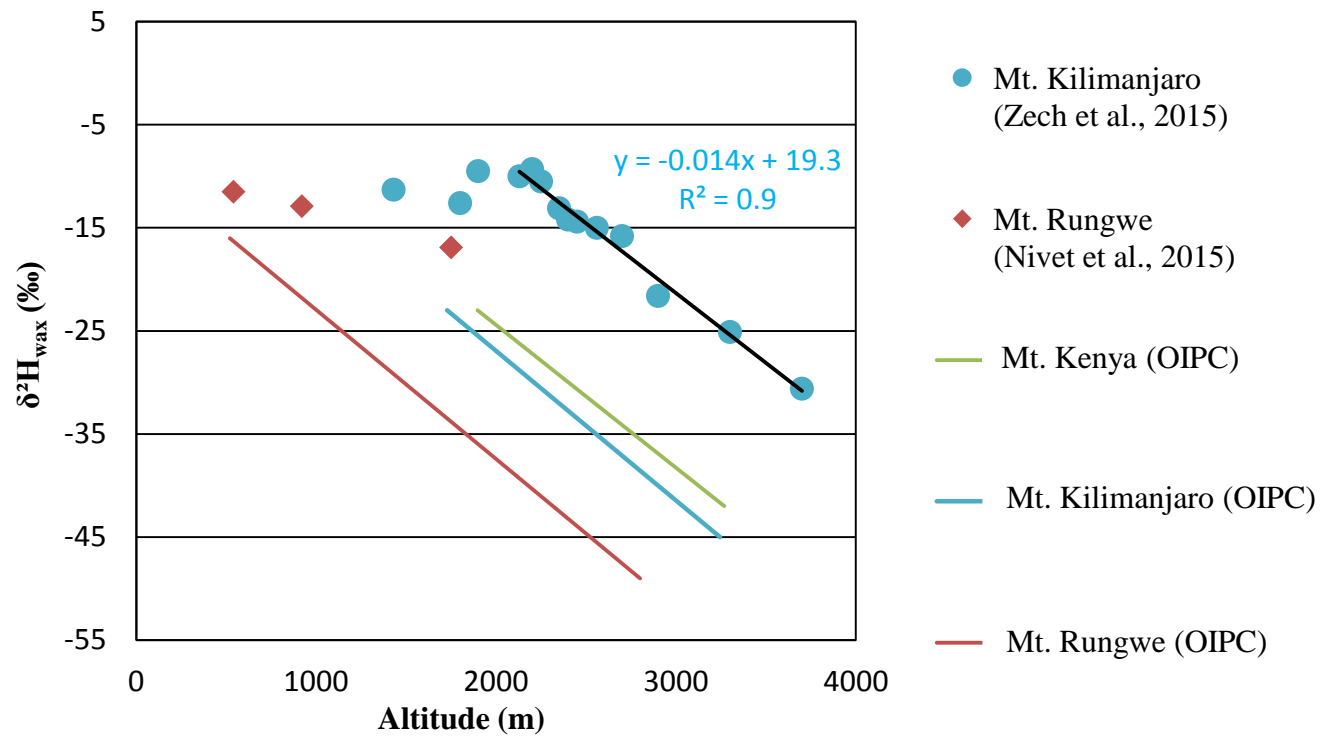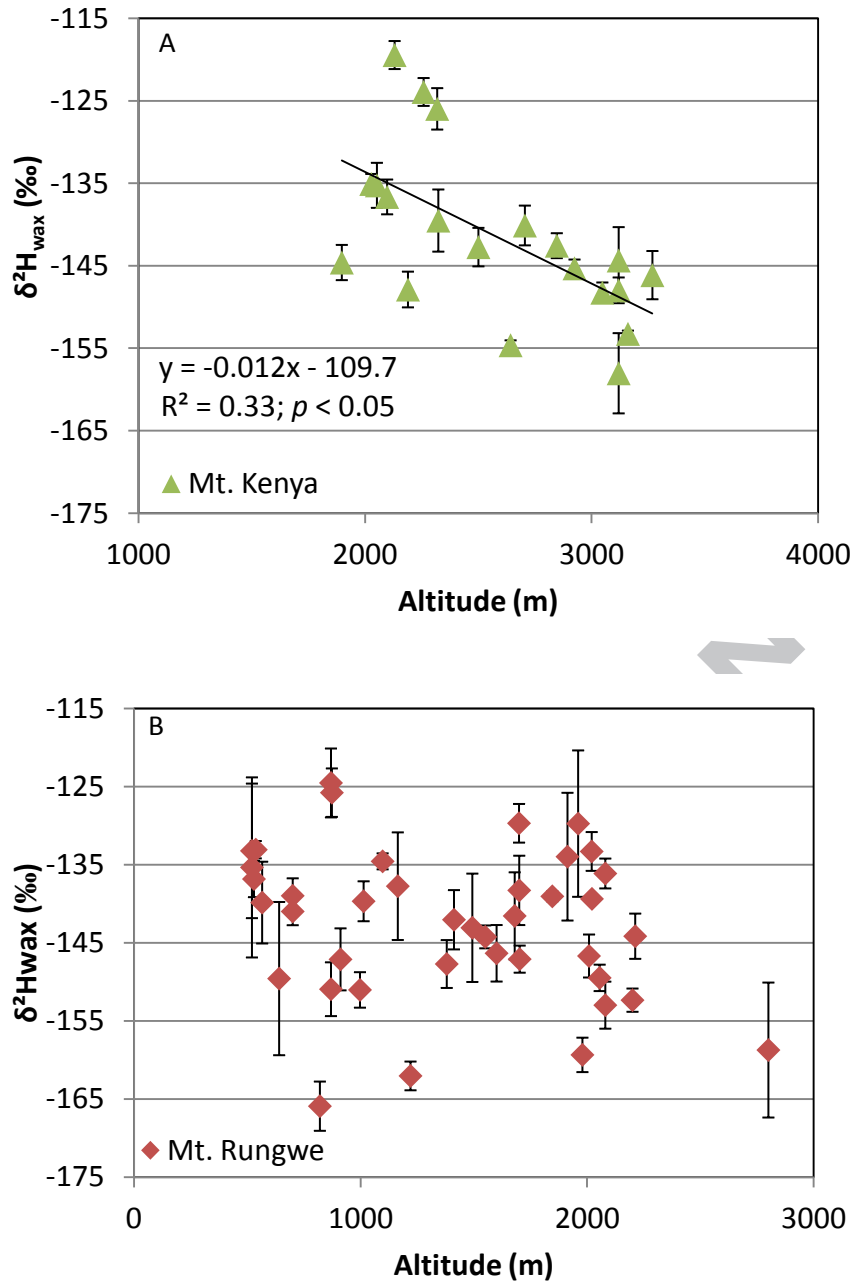
720

721

27

Figure 1.

Figure 2.

Figure 3.

Figure 4.

Global soil MBT/CBT calibration

New East African soil MBT/CBT calibration
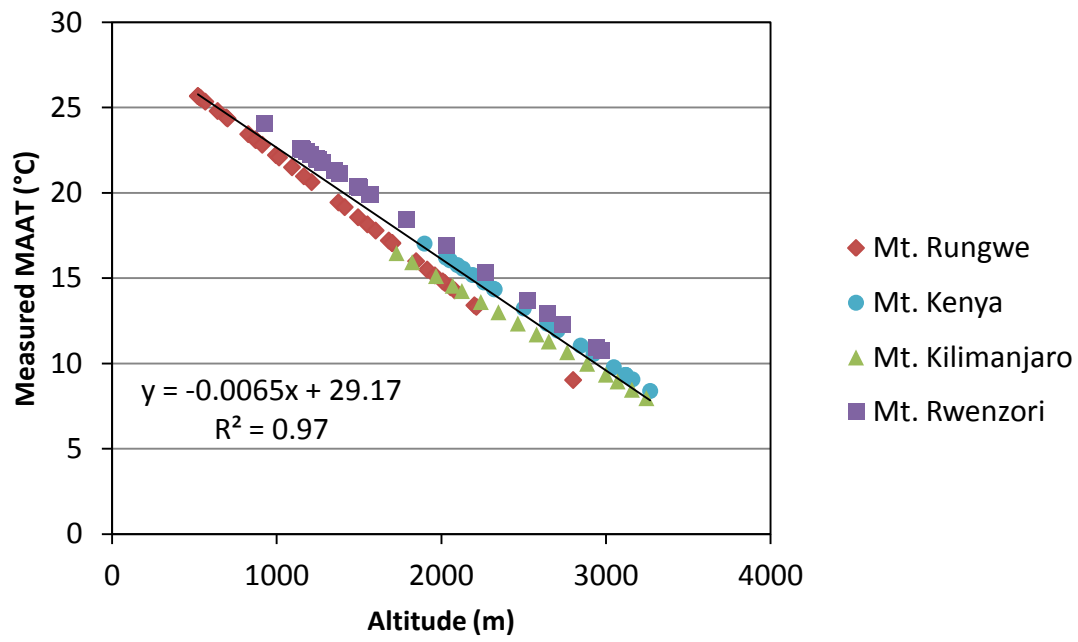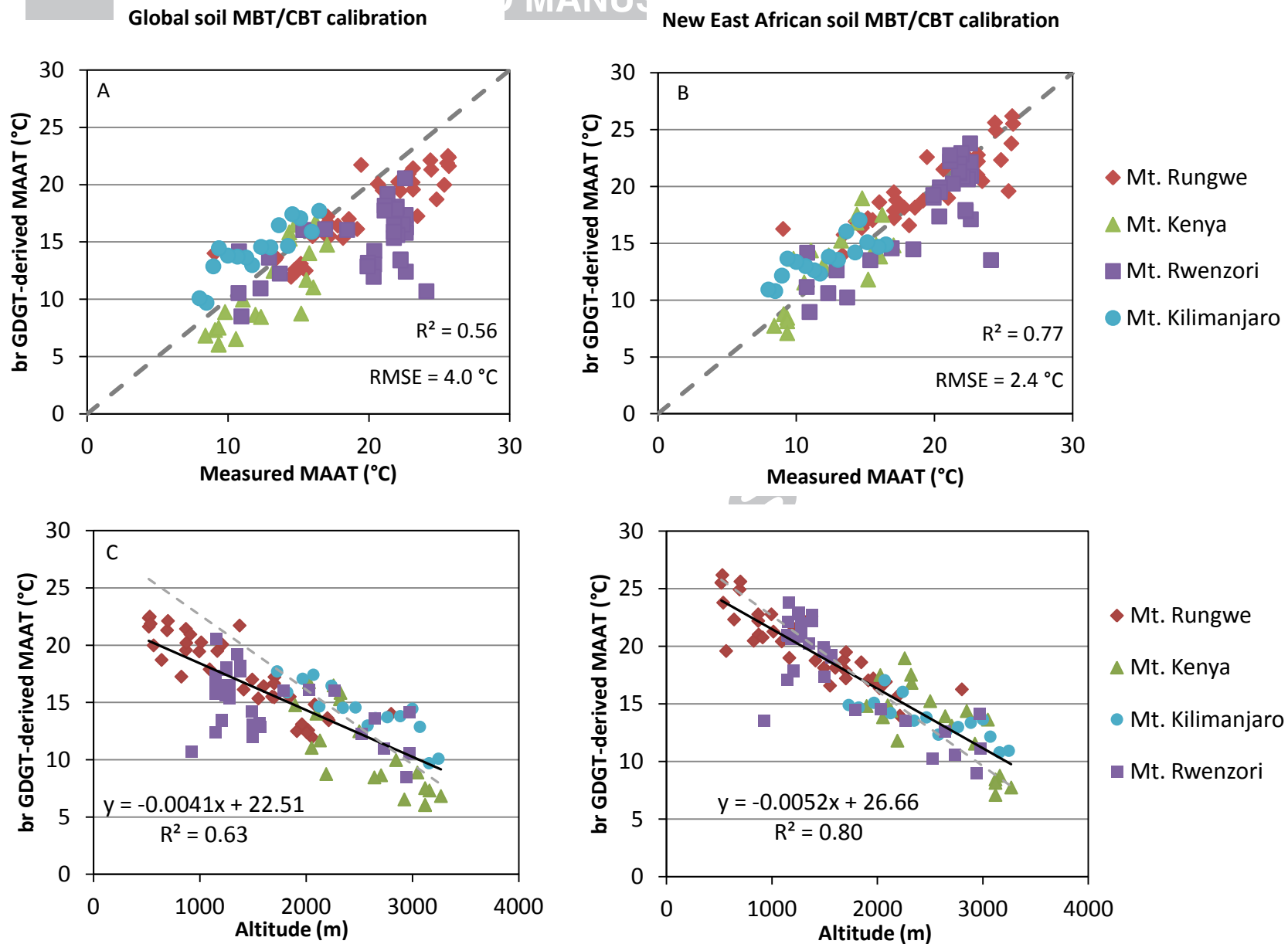
Figure 5.

722

723 **Table 1.**

724

camp.	n°	altitude (m.a.s.l.)	MAAT (Peterse et al.. 2012)	MAAT (this study)	δ²H$_{wax}$[a] (‰)	camp.	n°	altitude (m.a.s.l.)	MAAT (Peterse et al.. 2012)	MAAT (this study)	δ²H$_{wax}$ (‰)	camp.	n°	altitude (m.a.s.l.)	MAAT (Peterse et al.. 2012)	MAAT (this study)	δ²H$_{wax}$ (‰)
Mt. Rungwe (2012)	1	520	21.6	25.9	-133±9	Mt. Rungwe (2014)	22	537	21.9	24.5	-133±1	Mt. Kenya (2013)	41	3160	10.0	9.6	-153±0
	2	520	22.4	26.0	-135±12		23	565	20.0	20.8	-140±5		42	3119	10.2	9.4	-148±2
	3	529	22.5	26.6	-137±2		24	700	22.1	26.1	-141±2		43	3119	10.2	8.9	-158±5
	4	640	18.7	22.8	-150±10		25	873	20.2	22.0	-126±3		44	3119	10.2	8.1	-144±4
	5	700	21.3	25.4	-139±2		26	911	20.9	21.9	-147±4		45	3268	9.3	8.7	-146±3
	6	820	17.3	21.0	-166±3		27	1013	20.2	22.2	-140±3		46	3047	10.3	13.9	-148±1
	7	869	19.6	22.8	-151±3		28	1164	19.5	20.2	-138±7		47	2924	11.7	11.8	-145±1
	8	869	21.4	23.6	-125±4		29	1412	16.1	19.4	-142±4		48	2846	11.9	14.7	-143±2
	9	997	19.5	23.3	-151±2		30	1493	17.0	19.0	-143±7		49	2705	13.0	13.4	-140±2
	10	1097	17.9	21.1	-135±1		31	1600	16.4	18.9	-146±4		50	2642	13.2	14.1	-155±1
	11	1220	20.1	22.3	-162±2		32	1699	16.7	18.8	-130±2		51	2500	13.8	15.9	-143±2
	12	1380	21.7	23.5	-148±3		33	1700	15.5	18.0	-138±4		52	2323	14.7	17.8	-140±4
	13	1550	15.4	17.5	-144±1		34	1913	12.5	17.3	-134±8		53	2189	15.5	12.4	-148±2
	14	1680	15.5	19.3	-142±6		35	1960	13.1	17.6	-130±9		54	2097	16.2	15.8	-137±2
	15	1702	17.2	20.2	-147±2		36	2008	12.4	17.0	-147±3		55	2052	16.4	14.5	-135±3
	16	1846	15.5	19.2	-139±1		37	2212	13.5	15.0	-144±3		56	1897	16.9	15.9	-145±2
	17	2020	12.8	16.8	-133±2		38	2080	n.a.[b]	n.a.	-136±2		57	2027	16.4	18.5	-135±1
	18	2055	12.2	17.1	-149±2		39	2021	n. a.	n.a.	-139±0		58	2130	15.8	15.0	-119±2
	19	2080	14.8	17.7	-153±1		40	1979	n.a.	n.a.	-159±2		59	2258	15.1	19.6	-124±2
	20	2200	13.6	16.5	-152±1								60	2318	14.9	18.2	-126±3
	21	2800	14.0	17.0	-159±9												

725 [a] the analytical error of at least duplicate measurements is given

726 [b] not analysed for GDGT content.

727

28